# Scandium effect on undercooling and dendrite morphology of Al-4.5wt% Cu droplets

**J. Valloton[1,*], A.-A. Bogno[1], H. Henein[1], D.M. Herlach[2] and D. Sediako[3]**

[1] Advanced Materials and Processing Laboratory, University of Alberta, Edmonton, Canada, T6G 1H9
[2] Institut für Materialphysik im Weltraum, Deutsches Zentrum für Luft- und Raumfahrt, Cologne, Germany, 51170
[3] UBC Okanagan, Kelowna, BC, Canada, V1V 1V7.

[*] Corresponding author: valloton@ualberta.ca

**Abstract**

This paper reports on the undercooling and growth morphology of Al-4.5wt%Cu and Al-4.5wt%Cu-0.4wt%Sc with a focus on the effect of Sc addition. It is found that the addition of Sc reduces the undercoolings of both primary phase and eutectic. In addition, the morphology of the Al-4.5wt%Cu-0.4wt%Sc dendrites is less favored in the <111> direction at similar undercoolings as with Al-4.5wt%Cu. The development of Solidification Continuous Cooling Transformation diagrams that relate the solidification paths to the inherent solidification microstructures is also introduced. The Solidification Continuous Cooling Transformation diagrams are obtained, based on the measurement of phase fractions of a solidified microstructure. The quantitative data is combined with well-established solidification models and phase diagrams to yield undercooling temperatures of individual phases. The thermal history and undercooling of different phases in the solidified alloy are estimated for a wide range of cooling rates (from $10^{-2}$ K/s to $10^{4}$ K/s). It is found that a minimum cooling rate of about 1 K/s is required to avoid the nucleation of the detrimental intermetallic, W-phase in hypo-eutectic Al-Cu-Sc.

## Introduction

Aluminum is the 3rd most abundant element on the planet, accounting for about eight percent of the Earth's crust. Aluminum alloys occupy an important place in various industrial applications, such as automotive and aerospace. This is due to their good mechanical properties coupled with low density (i.e. excellent strength-to-weight ratio), corrosion resistance and castability [1]. Aluminum alloys are typically strengthened via precipitation of secondary intermetallic phases from alloying elements in solid solution. Copper is one of the most widely used alloying element due to its well-known age hardening effect characterized by precipitation of finely dispersed Guinier–Preston (GP) zones, θ' and followed by the stable θ phase through heat treatment [2].

Lately, the development of commercial age-hardenable aluminum alloys with improved performances has focused on systems forming $Al_3X$ precipitates, such as Al-Sc, Al-Zr or Al-V [3]. Of these, Al-Sc alloys have garnered the most attention [4][5]. Age hardening leads to the formation of a dense and homogeneous dispersion of approximately spherical $Al_3Sc$ particles. These nanosized precipitates effectively block the movement of dislocations and grain boundaries and thus stabilize fine-grained structures [5][6][7]. Besides precipitation hardening, addition of Sc to Al-alloys can also act as a grain refiner during casting using hypereutectic additions of Sc. Indeed, $Al_3Sc$ has an FCC structure and a lattice parameter close to that of α-Al [8]. For hypereutectic compositions of Sc, $Al_3Sc$ precipitates will thus act as nuclei for the formation of the aluminum phase [9].

Ternary Al-Cu-Sc alloys have been scarcely studied. In addition to the traditional $Al_2Cu$ and $Al_3Sc$ intermetallics, Kharakterova reported one ternary compound, $Al_{8-x}Cu_{4+x}Sc$ ($0 \leq x \leq 2.6$), that can be in equilibrium with α-Al [10][11]. This phase, dubbed W-phase, is found in the Al-rich corner of the Al–Cu–Sc phase diagram, as shown in Figure 1. Recently, Bo et al. carried out a thermodynamic analysis of this system [12]. A good agreement was found between calculated phase equilibria and the reported experimental data from Kharakterova. The W-phase was further evidenced in the work of Bogno et al. during solidification of Al-4.5wt%Cu-0.4wt%Sc at low cooling rates [7]. Their work showed that the addition of 0.4wtSc to Al-4.5wt%Cu did not demonstrate any significant benefit since most of the Sc precipitated as the W-phase. Only a slight hardness increase was observed after heat treatment, which was attributed to the precipitation of the remaining Sc in solid solution within the matrix to form $Al_3Sc$. In general, the formation of the W-phase is detrimental as it consumes part of the Sc and Cu atoms in the Al matrix. As a consequence, both the precipitation of $Al_3Sc$ and the occurrence of Cu strengthening phases are reduced and this minimizes the positive effect of Sc on the mechanical properties of the alloy [13].

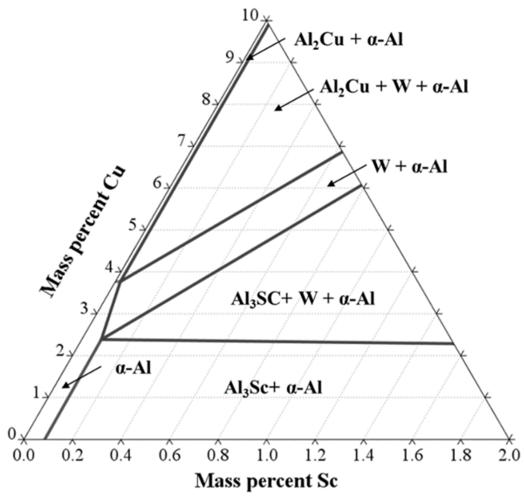


**Figure 1:** Isothermal section of the Al-rich corner of the Al-Cu-Sc system at 500°C computed with Thermocalc [14] using the ALDEMO database.

Our previous study of rapidly solidified Al-4.5wt%Cu and Al-4.5wt%Cu-0.4wt%Sc samples showed that with hypoeutectic additions of Sc in Al-4.5wt% Cu, no grain refining effect is observed [15]. Furthermore, rapid solidification supersaturates copper and scandium in the aluminum matrix and in the interdendritic regions, and thus prevents the formation of the W-phase. A dramatic improvement in mechanical properties is observed when Al-4.5wt%Cu-0.4wt%Sc samples are aged, with the microhardness increasing from about 75 HV as-atomized to 120 HV after heat treatment. This is attributed to the precipitation of nanosized $Al_3Sc$ and $Al_2Cu$ particles. Thus, by rapidly solidifying Al-4.5wt%Cu-0.4wt%Sc, the solutionizing and quenching step can be omitted from the regular heat treatment process.

As scandium remains a very expensive alloying element, keeping its level low is economically warranted. This work thus reports on the solidification of Al-4.5wt%Cu containing 0, 0.2 and 0.4wt%Sc under cooling rates varying from $10^0$ K/s to $10^4$ K/s by Differential Scanning Calorimetry (DSC), Electro-Magnetic Levitation (EML) and Impulse Atomization (IA). This paper focuses on the effect of Sc on the undercooling and the morphology of the solidified samples and introduces Solidification Continuous Cooling Transformation (SCCT) diagrams for Al-4.5wt%Cu and Al-4.5wt%Cu-0.4wt%Sc.

## Experimental methods

Impulse atomization (IA) is a drop tube-type containerless solidification technique where solidifying droplets experience high cooling rates and nucleation undercoolings [16]. It consists in the transformation of a bulk liquid into a spray of liquid droplets that solidify rapidly during free fall by losing heat to a surrounding gas of choice (usually $N_2$, Ar or He). The base material is melted using an induction furnace and the atomization is achieved by the application of a mechanical pressure (impulse) to the melt in order to push it through a nozzle plate with one or several orifices of known size and geometry. A liquid ligament emanates from each orifice, which in turn breaks up into droplets due to Rayleigh-type instabilities. The solidified powders are then collected in a beaker at the bottom of the tower. IA generates a range of droplets sizes per run, giving a range of cooling rates and undercoolings. The cooling rate is a function of both the droplet size and the gas in the atomization tower and can reach up to ~$10^5$ K/s. However, no direct measurement of temperature has been feasible to date. The cooling rates of individual droplets are estimated using a solidification model for atomization developed by Wiskel et al. [17][18] while primary and secondary phase nucleation undercoolings are determined using a new, novel methodology described in details in [19], with a summary given below.

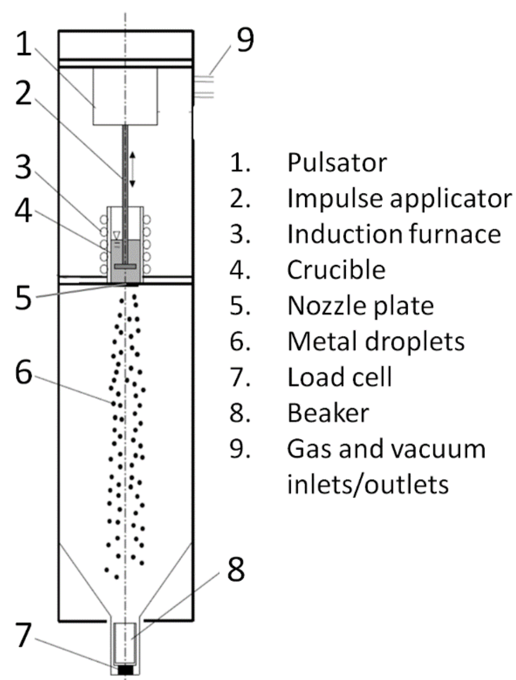


**Figure 2:** Schematic view of an impulse atomization apparatus.

The methodology is based on experimental determination of phase fraction using Neutron Diffraction. The eutectic fraction is determined from the fraction of $Al_2Cu$ obtained by Rietveld refinement of the diffraction spectra for an Al-Cu alloy (Figure 3 left) [20]. The corresponding eutectic nucleation undercooling is then evaluated from the metastable extension of the solidus and liquidus of the phase diagram of the alloy (Figure 3 right). The primary dendritic nucleation undercooling is subsequently determined using semi-empirical coarsening models of secondary dendrite arms. In the case of Al-4.5wt%Cu-0.4wt%Sc, the same methodology was used with a pseudo-binary phase diagram generated with ThermoCalc.

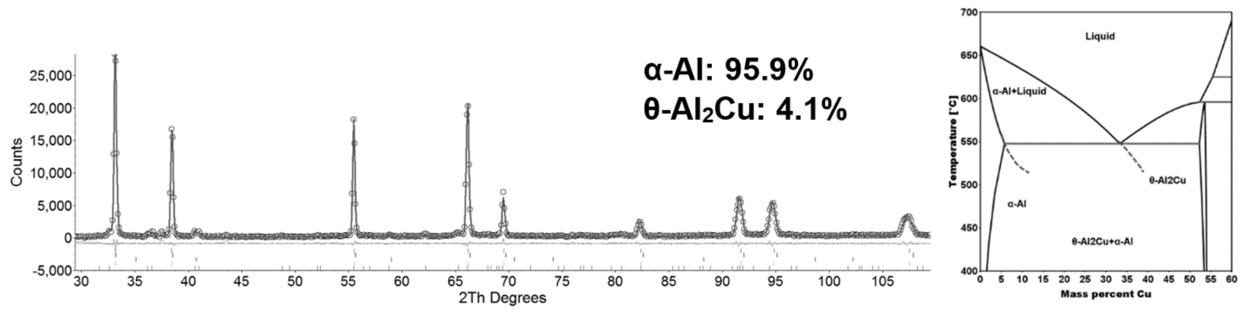


**Figure 3:** Left: Neutron diffraction diagram of IA droplets of Al-4.5wt% Cu. The phase fractions are obtained by Rietveld refinement analysis of the diffraction pattern. Right: Al-richer corners of Al-Cu binary phase diagrams. The dashed lines represent the extensions of the solidus and liquidus lines obtained with ThermoCalc using the TTAL7 database.

Electromagnetic levitation (EML) is a powerful containerless solidification technique for the processing of metallic and semiconductor samples with a large range of undercoolings. A schematic view of the apparatus is shown in Figure 4. An alternating current flowing through a water-cooled levitation coil produces an alternating electromagnetic field. A conducting sample placed within this field is levitated by the Lorentz force $F_L$ which compensates for the gravitational force $F_G$. Simultaneously, the eddy currents induced in the sample heat and melt the sample by ohmic losses. To solidify the sample, cooling jets of inert gas are used. The temperature of the sample is monitored continuously with a two-color pyrometer (Impac IGA10-LO) with an accuracy of ±5 K. As shown in Figure 4, this allows for a direct measurement of undercoolings, as well as cooling rates. Detailed information on the EML technique can be found in [21].

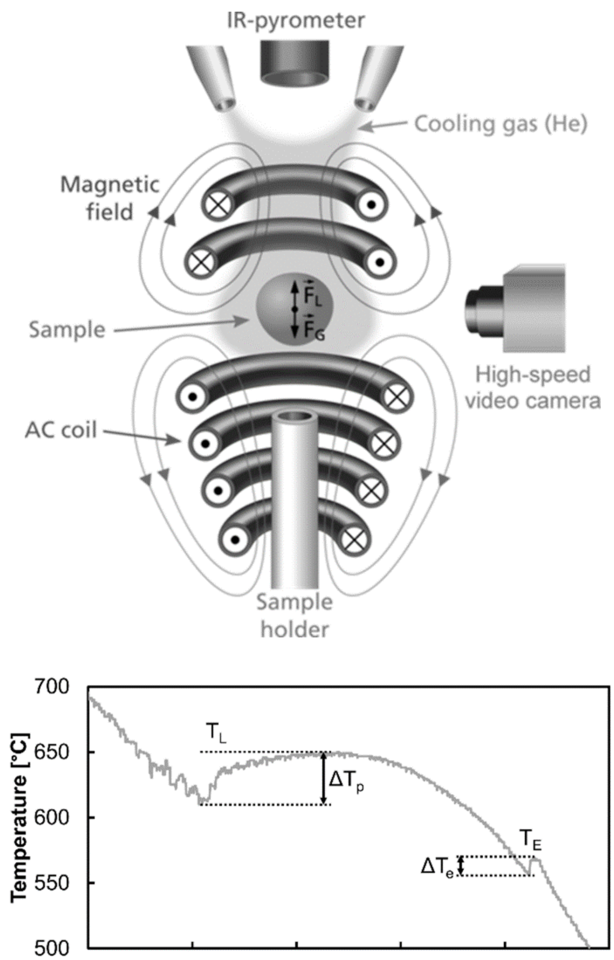


**Figure 4:** Schematic view of an EML apparatus and typical temperature-time profile obtained during EML solidification of an Al-4.5wt%Cu sample. Primary and eutectic solidification are clearly identified by the corresponding recalescence events of undercoolings $\Delta T_p$ = 34 K and $\Delta T_e$ = 13 K respectively.

DSC is a thermal analysis technique used to determine the amount of energy absorbed or released by a sample as it is heated or cooled in a controlled manner inside a crucible. As a non-containerless solidification technique, it yields low nucleation undercooling and its cooling rate (measureable) is limited to a narrow range (50 K/s maximum). In this work Al-Cu and Al-Cu-Sc alloys were solidified under low cooling rates and low undercooling conditions in a Setaram Labsys Evo 1600 DSC using alumina crucibles. A typical solidification curve using DSC is presented in Figure 5. The nucleation temperatures can be inferred from the onset of the exothermic peaks. Along with the primary and eutectic peaks, the Al-4.5wt%Cu-0.4wt%Sc sample shows a third peak corresponding to the formation of the W-phase. Note that the difference in heat flows stems from the different masses of the two samples analyzed.

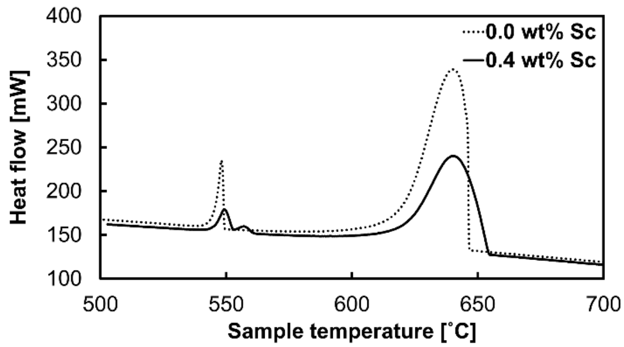


**Figure 5:** DSC solidification curves of Al-4.5wt%Cu and Al-4.5wt%Cu-0.4wt%Sc cooled at 5 K/min.

For metallographic analysis, DSC, EML and IA samples were first mounted in epoxy resin. Grinding was carried out using silicon carbide papers up to grit 1000 (P2500), followed by mechanical polishing with 3 and 1 μm diamond particles on soft cloths. Final polishing was performed with a 0.05 μm colloidal silica. Microstructural characterization was carried out using scanning electron microscopy (SEM) with a Zeiss Sigma FE-SEM running at 20 kV. Cell spacing measurements were obtained using the line intercept method on selected SEM micrographs according to ASTM E112-13.

Neutron diffraction measurements on IA samples were performed on the C2 neutron diffractometer located at the Canadian Neutron Beam Centre in Chalk River, Canada. Measurements were performed using a wavelength of 1.33 Å from a Si531 monochromator at 92.7° 2θ.

Synchrotron X-ray micro-tomography was carried out post-mortem at ESRF (European Synchrotron Radiation Facility, Grenoble, France) on the ID19 beamline. Two pixel resolutions were used: a high resolution of 0.18 μm/voxel (field of view of 369 μm side cube) to analyze in detail the fine microstructure of small droplets, and a medium resolution of 0.56 μm/voxel (field of view of 1146 μm side cube) to scan several small droplets at the same time to derive statistical data.

## Results and discussion

Cubic type crystals of metallic alloys such as Al-Cu, Al-Fe and Al-Ni generally grow along <100> directions due to the anisotropy of the solid-liquid interfacial energy. Under certain conditions (e.g. high undercooling) dendrites growth deviates from <100> and unusual and complex morphologies can develop. For example, in Al-0.6wt%Fe and Al-1.9wt%Fe impulse atomized droplets, a change in dendrite growth direction from <100> to <111> was observed [22]. For IA Al-4.5wt%Cu droplets, an earlier in-depth investigation by Bedel et al. [23] revealed four distinct dendritic morphologies using X-Ray microtomography (Figure 6). The highly branched morphology (a) shows dendrite growing along the usual <100> while microstructural features indicate that dendrite arms develop mostly along <111> directions in the other three morphologies (b-d). The transition from <100> to <111> is attributed to an increase in the solidification growth velocity. At the slowest solidification growth velocity, <100> arms develop (a). At higher cooling rates and/or undercooling, primary arms start growing along <111> but higher level arms forming after recalescence are slower and thus grow along <100> (b). At even higher solidification rates, the droplet solidifies completely with a <111> growth direction, as illustrated in (c). Finally, at the highest speed, a competition between different <111> arms originating from the same nucleation point leads to the formation of so-called finger bundles (d). Our collaborative work also showed that as the cooling rate increases, <111> dendrites are favored and the number of droplets with a finger bundle morphology increases.

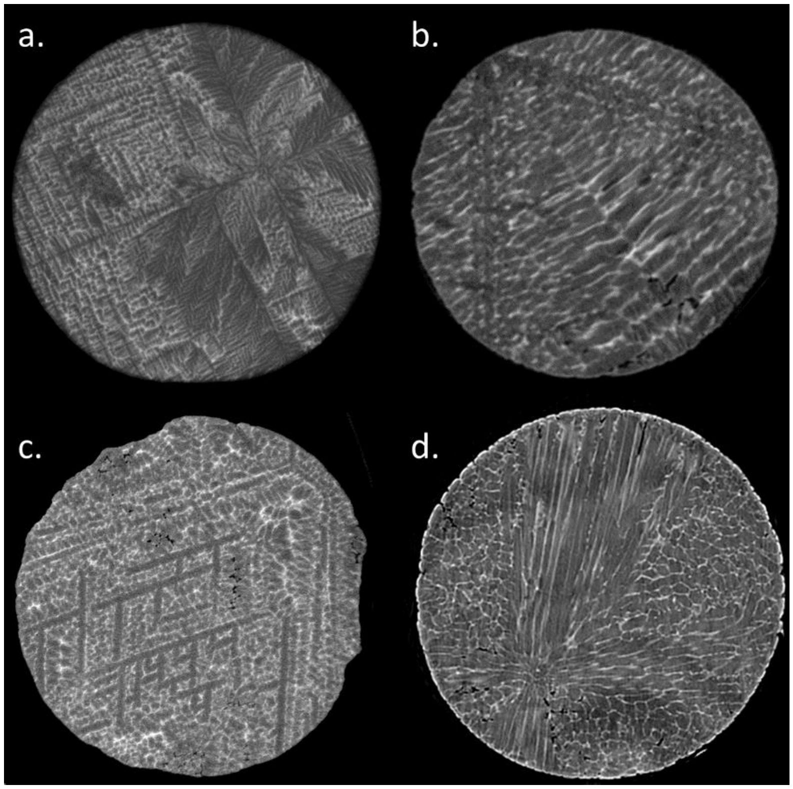


**Figure 6:** Typical dendrite morphologies observed in Al-4.5wt%Cu droplets solidified in IA: (a) <100> highly branched dendrites; (b) <111> to <100> dendrite transition; (c) <111> dendritic morphology; (d) <111> finger bundle morphology.

Figure 7 shows the statistical distribution of the four dendrite morphologies observed in IA droplets of composition Al-4.5wt%Cu and Al-4.5wt%Cu-0.4wt%Sc solidified in argon with diameters in the range of 0 to 212 μm. A total of 69 droplets were analyzed for Al-4.5wt%Cu and 91 for Al-4.5wt%Cu-0.4wt%Sc. When Sc is added, it is observed that the number of droplets with finger bundles decreases in favor of lower speed morphologies. As the processing gas and the droplet size range are the same in both cases, the droplet cooling rates are expected to be similar, regardless of the presence of scandium. Thus, this shift in morphology is attributed to a change in the droplet undercoolings induced by the addition of Sc, as will be discussed later.

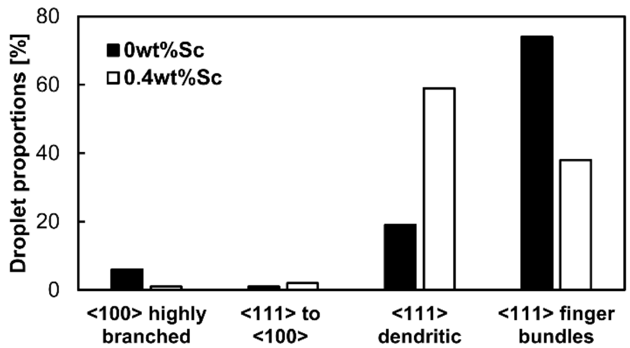


**Figure 7:** Statistical distribution of the four morphologies in Al-4.5wt%Cu and Al-4.5wt%Cu-0.4wt%Sc droplets Impulse Atomized in Ar with a diameter range 0<d<212 μm.

Figure 8 shows a representative solidification microstructure of an Al-4.5wt%Cu sample solidified in EML with a solidification cooling rate of ~9 K/s and primary and eutectic undercoolings of $\Delta T_p$ = 34 K and $\Delta T_e$ = 13 K, respectively, as well as an Al-4.5wt%Cu-0.4wt%Sc sample solidified at ~12 K/s with $\Delta T_p$ = 6 K and $\Delta T_e$ = 4 K. EML samples typically show a cellular microstructure with no obvious growth direction. Some dendritic remnants can be observed in Figure 8 and in other EML samples. When present, these dendrites exhibit <100> growth direction in all cases. This suggests that the growth velocity in EML samples is slower than in IA. This is supported by the scale of the microstructure, which is one order of magnitude coarser in EML than in IA samples. Finally, it is observed that the addition of scandium does not alter the morphology of the solidified EML samples.

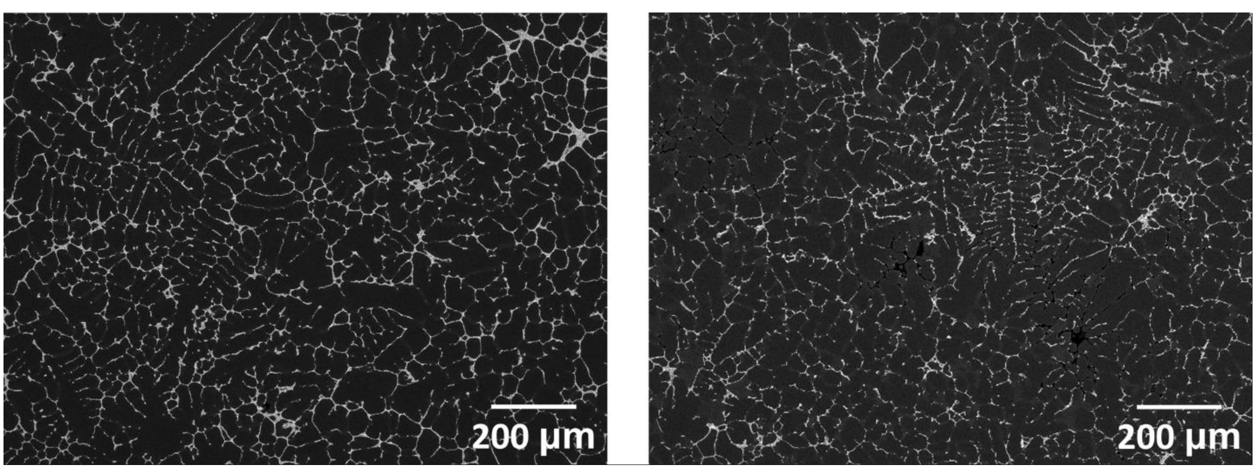


**Figure 8:** Representative solidification microstructure of Al-4.5wt%Cu solidified in EML at ~9 K/s with $\Delta T_p$ = 34 K and $\Delta T_e$ = 13 K (left) and Al-4.5wt%Cu-0.4wt%Sc solidified in EML at ~12 K/s with $\Delta T_p$ = 6 K and $\Delta T_e$ = 4 K (right). In both cases, the structure is mostly cellular with some dendrite remnants showing <100> growth directions.

Figure 9 shows the cell spacing measured with the line intercept methods as a function of cooling rate for DSC, EML and IA samples [15]. Regardless of the solidification technique, the effect of Sc addition on the microstructures scale is found to be negligible. However, microstructure refinement is shown to be very dependent on the cooling rate. This relationship follows a power law of the type $\lambda_2=A\dot{T}^{-n}$, where $\lambda_2$ is the cell spacing, $\dot{T}$ the cooling rate and A and n are constants, as described by Eskin et al. [24]. The values of A and n found in this study are in the range of values published by Mullis and co-workers in the estimation of cooling rates during close-coupled gas atomization of Al-4wt%Cu using secondary dendrite arm spacing measurements [25]. Furthermore, the exponent value being very close to the theoretical value of 1/3 [26], the decrease in cell spacing observed with increasing cooling rate indicates that the final scale of the microstructure is governed mainly by coarsening.

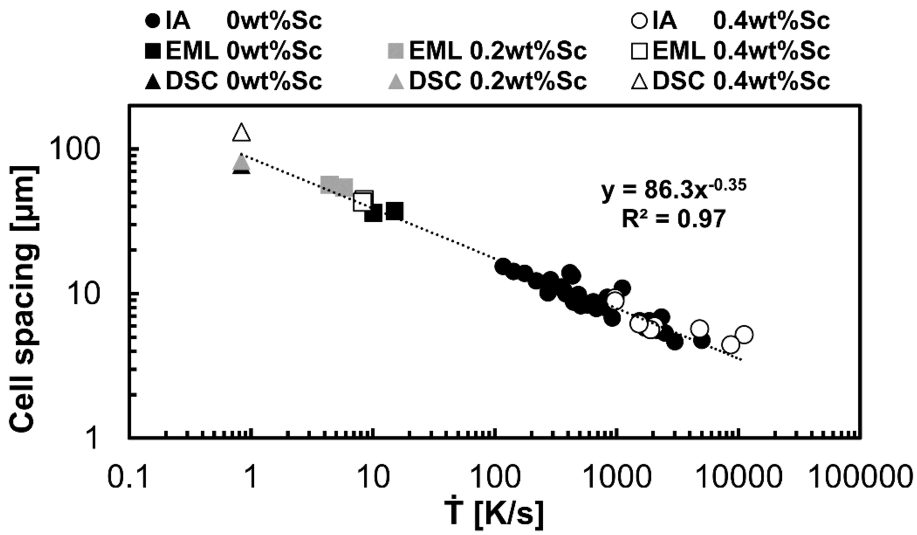


**Figure 9:** Variation of cell spacing with cooling rate for Al-4.5 wt% Cu with different Sc levels.

As EML experiments allow the direct measurement of the temperature profile during solidification, it is easy to assess the effect of scandium addition on the nucleation behavior of the alloy studied. Table 1 compiles the average of the measured undercoolings obtained during EML solidification of Al-4.5wt%Cu samples with the addition of 0, 0.2 and 0.4wt%Sc (9, 7 and 12 solidified samples respectively). Nucleation being a stochastic event, a range of undercoolings is obtained for each composition, which is reflected in the standard deviation for each composition in Table 1. It is clear that the addition of Sc promotes the nucleation of the $\alpha$-Al and $\theta$-$Al_2Cu$ phases as both the primary and eutectic undercoolings decrease when Sc is added to the alloy. The primary undercooling decreases significantly only with a 0.4wt%Sc addition, while both 0.2 and 0.4wt%Sc exhibit the same change in eutectic undercooling. This suggests that the presence of scandium in the melt is sufficient to alter the interfacial energy between the Sc containing liquid and $Al_2Cu$ and to promote nucleation of the intermetallic phase. The results of cooling rate of the liquid samples, as well as the primary and eutectic undercoolings for each method used is presented in Figure 10. The same trend is observed, regardless of the cooling rate or solidification technique.

**Table 1:** Average primary and eutectic nucleation undercoolings during EML solidification.

| | $\Delta T_p$ [K] | $\Delta T_e$ [K] |
|---|---|---|
| **0 wt% Sc** | 35.7 ± 6.5 | 10.1 ± 1.9 |
| **0.2 wt% Sc** | 30.9 ± 6.4 | 3.6 ± 0.9 |
| **0.4 wt% Sc** | 13.8 ± 5.7 | 3.7 ± 1.8 |

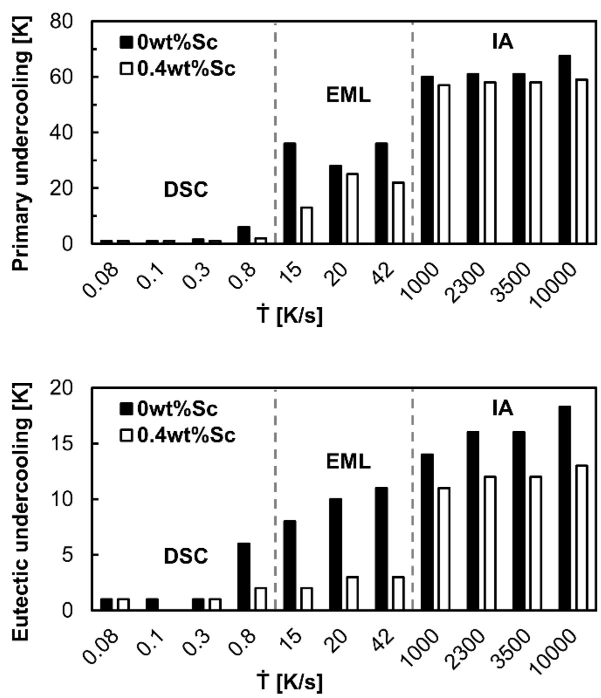


**Figure 10:** Variation of nucleation undercooling with solidification cooling rate for Al-4.5wt%Cu and Al-4.5wt%-0.4wt%Sc

As reported in a previous contribution, X-ray and Neutron Diffraction of EML and IA samples did not show the presence of the W-phase. Only in the DSC solidified samples was the W-phase observed [7]. Knowing this, and with the results presented above, the quantification of the solidification path of Al-4.5wt%Cu and Al-4.5wt%Cu-0.4wt%Sc alloys is possible. In order to represent the resultant microstructure and relate it to macro-solidification conditions, solidification continuous cooling transformation (SCCT) curves were developed. To construct these maps, the liquid cooling rates of the samples were used (imposed for DSC, measured on the temperature-time profile for EML, and estimated with the atomization model for IA) and the corresponding undercoolings from Figure 10 were plotted on a CCT diagram (Figure 11 and 12). Also plotted on these diagrams are the equilibrium liquidus, $T_L$, and eutectic, $T_E$, of the respective alloys. From these results, it is observed that both primary phase and eutectic nucleation undercoolings increase as the cooling rate is increased. Also, to avoid the formation of the detrimental ternary W-phase, a cooling rate of the order of 1 K/s is necessary.

The use of the SCCT diagrams is not restricted to solidifying liquid droplets but should apply to any liquid of the Al-4.5wt%Cu-(0.4wt%Sc) composition solidifying in any given solidification process. Limitations to the use of this diagram will occur when there is significant segregation of Cu during solidification. However, in these instances, similar SCCT diagrams may be derived using droplet cooling rates for alloys with different Cu compositions, to trace the path of solidification of a given alloy in a particular process. This is the subject of further research.

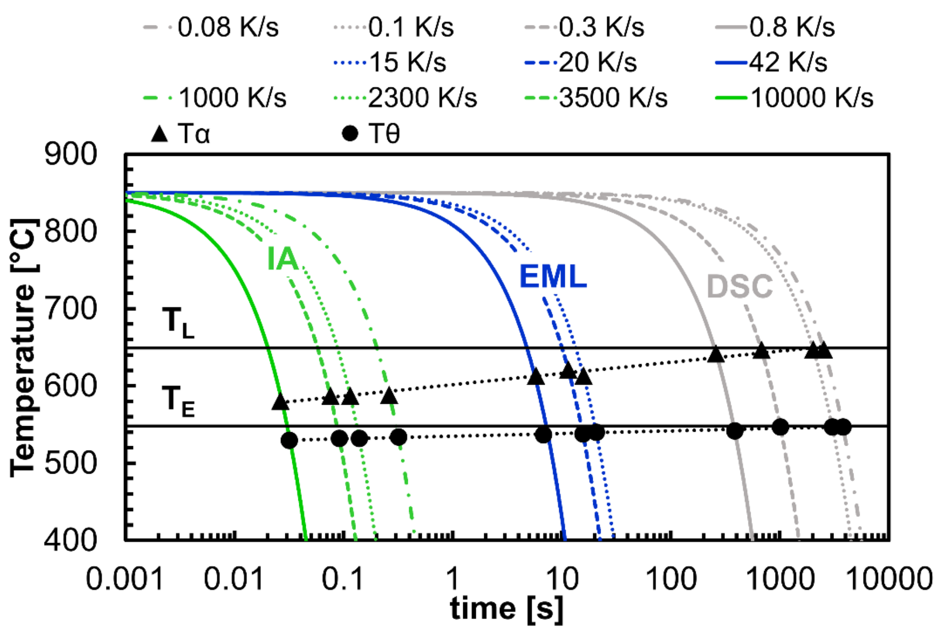


**Figure 11:** Solidification Continuous Cooling Transformation curves of Al-4.5wt%Cu

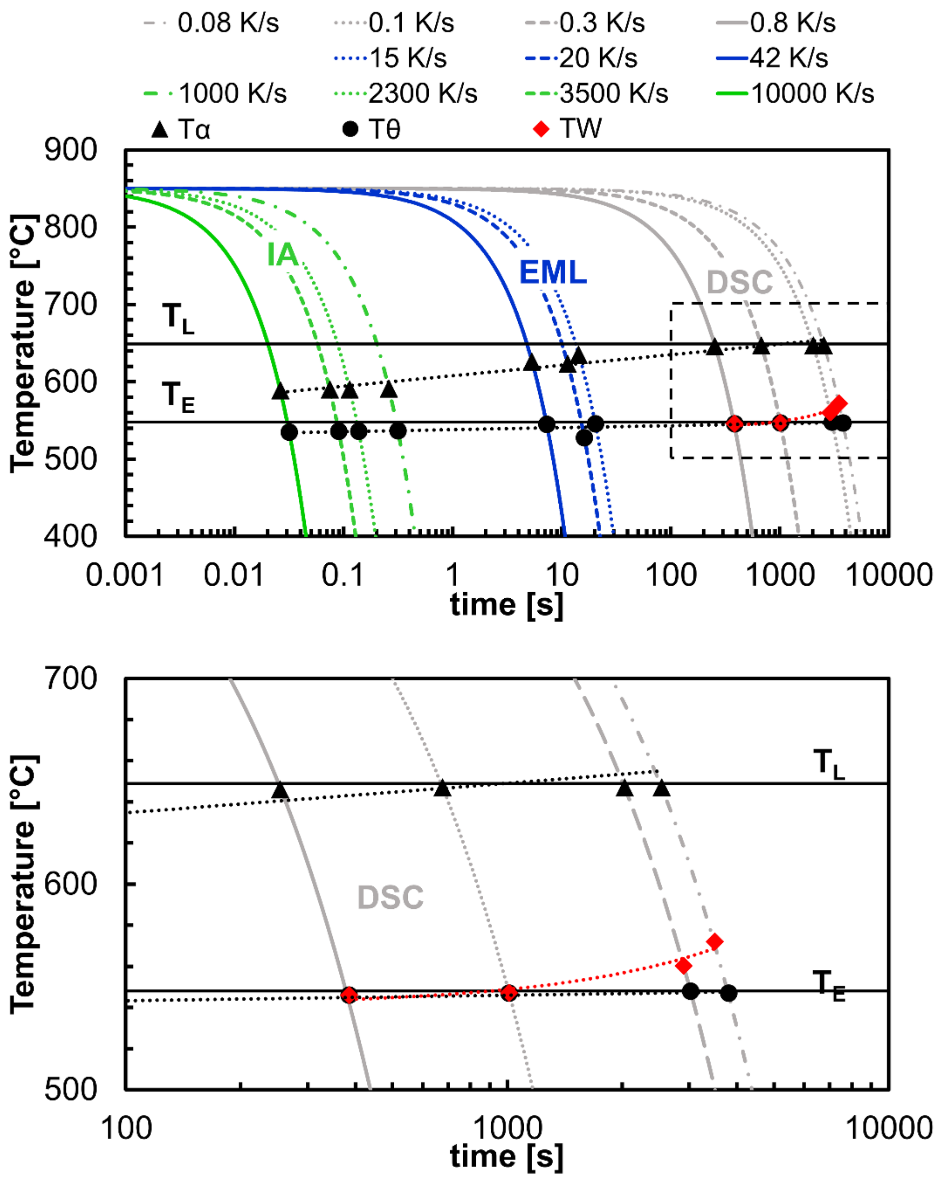


**Figure 12:** Top: Solidification Continuous Cooling Transformation curves of Al-4.5wt%Cu-0.4wt%Sc. Bottom: Magnified view of the nucleation temperatures of the ternary W-phase.

## Conclusions

Al-4.5wt% Cu with different level of Sc addition (0, 0.2 and 0.4wt%) were generated under low, medium and high cooling rate conditions respectively by DSC, EML and IA. No refining effect of Sc is found. Cell spacing variation with cooling rate for the investigated alloys is found to follow an empirical coarsening law of secondary dendrite arms spacing commonly found in literature. Sc addition is shown to reduce both the primary and eutectic undercoolings in all three types of solidification experiments carried out. This in turns promotes the formation of lower speed morphologies as evidenced by the decrease of droplets exhibiting finger bundles in IA samples.

Using solidification continuous cooling transformation maps, the solidification path of Al-4.5wt%Cu and Al-4.5wt%Cu-0.4wt%Sc has been charted over a wide range of cooling rates. An increase in cooling rate leads to an increase of the primary and eutectic undercoolings. During DSC experiments at low cooling rates, scandium induces the precipitation of the W-phase, which is detrimental to the mechanical properties of the alloy. At higher cooling rates in EML and IA, the precipitation of the W-phase is suppressed. The SCCT diagram shows that a minimum cooling rate of about 1 K/s is required to avoid the nucleation of the detrimental intermetallic, W-phase.

**Acknowledgements**

Financial support from the Natural Sciences and Engineering Research Council of Canada (NSERC) and the European Space Agency (ESA) within the frame of the NEQUISOL project is gratefully acknowledged. The authors are grateful to the Canadian Nuclear Laboratories (CNL) and the European Synchrotron Radiation Facility (ESRF) for beam time and expert support during the measurement campaigns. The assistance of Daniel Auras with morphology analysis is appreciated.

**References**

[1] J.R. Davis (ed.): *ASM Specialty Handbook: Aluminum and Aluminum Alloys*, ASM International 1993.

[2] P. Haasen: *Physical Metallurgy*, 3rd ed., Cambridge University Press, Cambridge, UK, 1996.

[3] Z.C. Sims, O.R. Rios, D. Weiss, P.E.A Turchi, A. Perron, J.R.I. Lee, T.T. Li, J.A. Hammons, M. Bagge-Hansen, T.M. Willey, K. An, Y. Chen, A.H. King and S.K. McCall: *Mater. Horiz.*, 2017, vol. 4 (6), pp. 1070-1078.

[4] N. Blake and M.A. Hopkins: *J. Mater. Sci.*, 1985, vol. 20 (8), pp. 2861-2867.

[5] D.N. Seidman, E.A. Marquis and D.C. Dunand: *Acta Mater.,* 2002, vol. 50 (16), pp. 4021-4035.

[6] L.S. Toporova, D.G. Eskin, M.L. Kharakterova and T.V. Dobatkina: *Advanced aluminum alloys containing scandium: structure and properties*, Gordon & Breach, Amsterdam, 1998.

[7] A.-A. Bogno, J. Valloton, H. Henein, D.G. Ivey, A.J. Locock, and M. Gallerneault: *Can. Metall. Quart.*, 2018, vol. 57 (2), pp. 148-159.

[8] J. Røyset and N. Ryum: *Int. Mater. Rev*., 2005, vol. 50 (1), pp. 19-44.

[9] J. Røyset: *Metall. Sci. Technol.*, 2007, vol. 25 (2), pp. 11-21.

[10] M.L. Kharakterova and T.V. Dobatkina: *Russ. Metal.*, 1988, vol. 6, pp. 175-178.

[11] M.L. Kharakterova: *Russ. Metal.*, 1991, vol. 4, pp. 191-194.

[12] H. Bo, L.B. Liu and Z.P. Jin: *J. Alloy. Compd.*, 2010, vol. 490 (1-2), pp. 318-325.

[13] S. Riva, K.V. Yusenko, N.P. Lavery, D.J. Jarvis and S.G.R. Brown: *Int. Mater. Rev*., 2016, vol. 61 (3), pp. 203-228.

[14] J.O. Andersson, T. Helander, L. Höglund L, S. Pingfang and B. Sundman: *Calphad*. 2002, vol. 26 (2), pp. 273-312.

[15] A.-A. Bogno, J. Valloton, H. Henein, M. Gallerneault and D.M. Herlach: in *Proc. 3rd Pan American Materials Congress*, Berlin, Springer, 2017, pp. 355-363.

[16] H. Henein: *Mater. Sci. Eng.*, 2002, vol. A326, pp. 92-100.

[17] J. Wiskel, H. Henein and E. Maire: *Can. Metall. Quart.*, 2002, vol. 41 (1), pp. 97-110.

[18] J. Wiskel, K. Navel, H. Henein and E. Maire: *Can. Metall. Quart.*, 2002, vol. 41 (2), pp. 193-204.

[19] A.-A. Bogno, P.D. Khatibi, H. Henein and Ch.-A. Gandin: *Metall. Mater. Trans. A*, 2016, vol. 47 (9), pp. 4606-4615.

[20] R. A. Young (ed.): *The Rietveld Method.* International Union of Crystallography/Oxford University Press, Oxford, UK, 1993.

[21] D. M. Herlach and D. M. Matson (eds.): *Solidification of Containerless Undercooled Melts*, 1st ed, Wiley-VCH, Weinheim, 2012, pp. 9-16.

[22] J. Chen, U. Dahlborg, C.M. Bao, M. Calvo-Dahlborg, and H. Henein: *Metall. Mater. Trans. B*, 2011, vol. 42 (3), pp. 557-567.

[23] M. Bedel, G. Reinhart, A.-A. Bogno, Ch.-A. Gandin, S. Jacomet, E. Boller, H. Nguyen-Thi and H. Henein: *Acta Mater.*, 2015, vol. 89, pp. 234-246.

[24] D. Eskin, Q. Du, D. Ruvalcaba and L. Katgerman: *Mater. Sci. Eng.*, 2005, Materials Science and Engineering A, 405 (1-2), pp. 1-10.

[25] A.M. Mullis, L. Farrell, R.F. Cochrane and N.J. Adkins: *Metall. Mater. Trans. B*, 2013, vol. 44 (4), pp. 992-999.

[26] J. A. Dantzig and M. Rappaz: *Solidification*, EPFL Press, Lausanne, 2009.